ALBERT-LUDWIGS-
UNIVERSITÄT FREIBURG

Termpaper

LHC and detectors

Author:
Fabian Schnell

Supervisor:
Dr. Markus
Schumacher

July 14, 2014

Contents

1 Introduction

Since decays particle physicists search for new particles in order to explain the structure of the universe. This has lead to the Standard Model theory, concerning the fundamental interactions such as electromagnetic, weak and strong nuclear interaction. In order to extend the Standard Model or to find physics beyond the Standard Model, particle colliders have been constructed over the course of time with increasing beam energies and luminosities for the purpose of finding new particles.
To date the researches have lead to the biggest particle collider worldwide, the LHC (*Large Hadron Collider*) which was built to search for the Higgs-boson and supersymmetry.
Two main experiments operate at the LHC to search for "new physics", the ATLAS (*A Toroidal LHC ApparatuS)* and CMS (*Compact Muon Solenoid)*)

2 LHC

2.1 General informations

The LHC is a two-ring-superconducting-hadron accelerator and collider. It is installed in the former LEP (*Large Electron Positron Collider*) tunnel, which has an circumference of 27.6km and is between 45m and 170m below earth's surface (see figure 2.1). The LHC is able to collide protons or Pb-ions. In the proton mode it operates with center-of-mass energies up to $E_{cms} = 14\text{TeV}$ and a luminosity $L = 10^{34}\text{cm}^{-2}\text{s}^{-1}$. Superconducting magnets deliver the needed 8.33T dipole field.

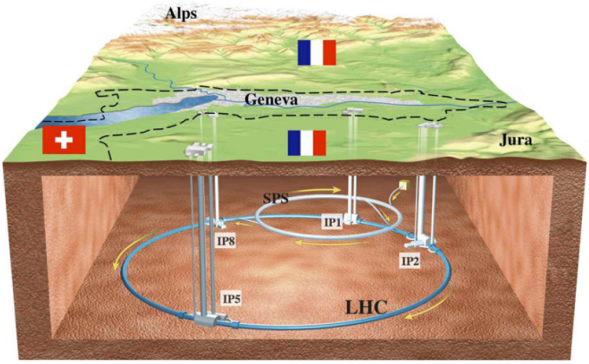

Figure 2.1: Sketch of the LHC below Geneva from [4]

2.2 LHC and Tevatron

Over the course of time the center-of-mass energies of the constructed particle colliders have been exponentially rising in order to find new particles. Before the LHC was built, Tevatron was the biggest hadron collider. The following figure (2.2) shows the development of the center-of-mass energy in different colliders over time.

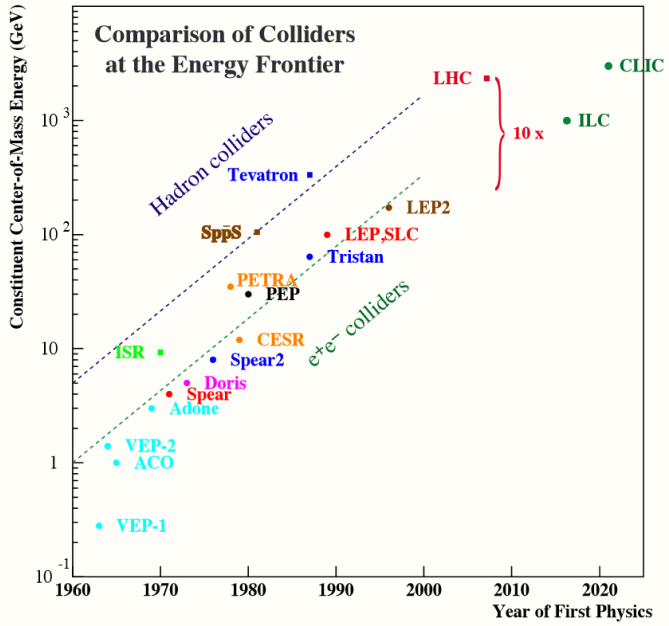

Figure 2.2: The graph shows the exponentially growth of the energy of different colliders (both hadron and e^+e^-) with time. Graph from [9]

The main difference between LHC and Tevatron is that

Tevatron is a proton-antiproton collider. The advantage of a $p\bar{p}$- collider is that the cross sections are higher than pp-colliders at low energies. However at high energies the cross sections are nearly similar because of confinement many new particle-antiparticle pairs are generated which leads to nearly equal collision conditions.
Besides the center-of-mass energy it is important to achieve sufficient large event rates. The event rate is given by:

$$\frac{dN}{dt} = L \cdot \sigma \tag{2.1}$$

with the luminosity L and any cross section σ.
For the higgs-boson cross sections between 10 and 10^4fb ($1\text{fb}=10^{-39}\text{cm}^2$) are expected (see figure 2.3). In order to grant sufficient large event rates for higgs discovery, a high luminosity is needed. Due to this the LHC was designed as a pp-collider because it is much easier to collect and collide protons than antiprotons.
Since high energies are needed to generate new particles hadron colliders are more suited for discoveries than e^+e^--colliders like LEP(2). Because of synchrotron radiation is it hardly possible to built high energy e^+e^- ring-colliders. But these colliders provide a higher precision than hadron colliders. Data from hadron colliders and e^+e^--colliders are used to complement each other. Table 2.1 compares the above-mentioned colliders LHC, LEP2 and Tevatron. Although the beam energies of LEP2 is magnitudes lower than LHC and Tevatron, the energy loss through synchroton radiation is magnitudes higher. LHC provides a luminosity of $10^{34}\text{cm}^{-2}\text{s}^{-1}$ and grants a sufficient large event rate for the Higgs search.

	LHC	LEP2	Tevatron
colliding beams of	p, p	e^+, e^-	$p, \bar{p}$
Momentum at collisions, TeV/c	7	0.1	0.98
Peak luminosity, $cm^{-1}s^{-2}$	10^{34} (design)	10^{32}	4.3×10^{32}
Dipole field at top energy, Tesla	8.33	0.11	4.4
Number of bunches, each beam	2808	4	36
Total beam current / beam, A	0.58	0.003	0.08
Particles / bunch, 10^{11}	1.15	4.2	2.9, 0.8
Typical beam size in the ring, μm	$200 - 300$	1800/140 (H/V)	500
Beam size at IP, μm	16	200 / 3 (H/V)	24
Fraction of energy lost in synchr.rad. per turn	10^{-9}	3%	10^{-11}
Total power radiated in synchr.rad., MW	0.0078	18	10^{-6}
Total energy stored in each beam, Megajoule	362	0.03	0.9
Total energy stored in the magnet system, Gigajoule	10	0.016	0.74

Table 2.1: Comparison between LHC, LEP2 and Tevatron. [9]

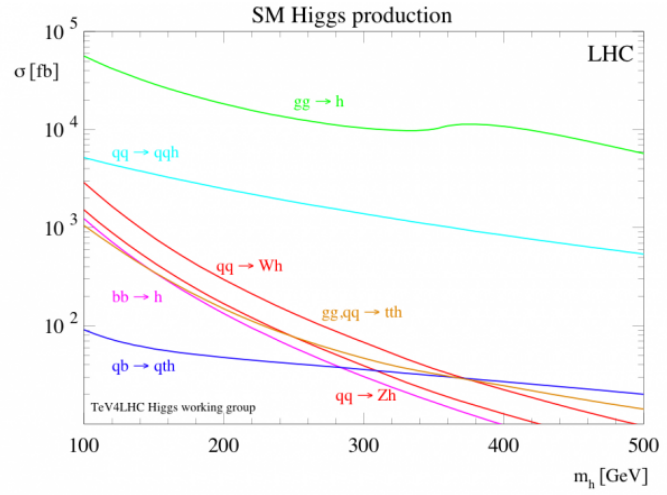

Figure 2.3: Cross section for different Higgs productions from [3]

3 Detectors

For measurements of the collisions at the LHC, several huge detectors have been built with different priorities. Two among them are dedicated to the search for new physics like Higgs or supersymmetry. The are called ATLAS and CMS.
This chapter will cover the structure of both detectors.

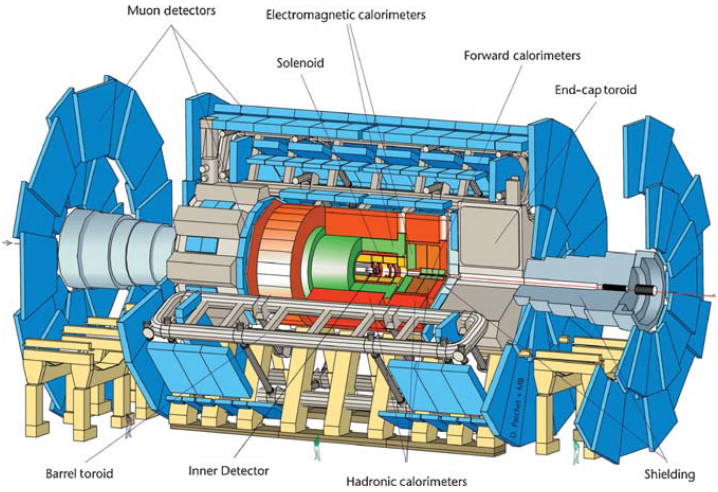

Figure 3.1: Structure of the ATLAS detector. [5]

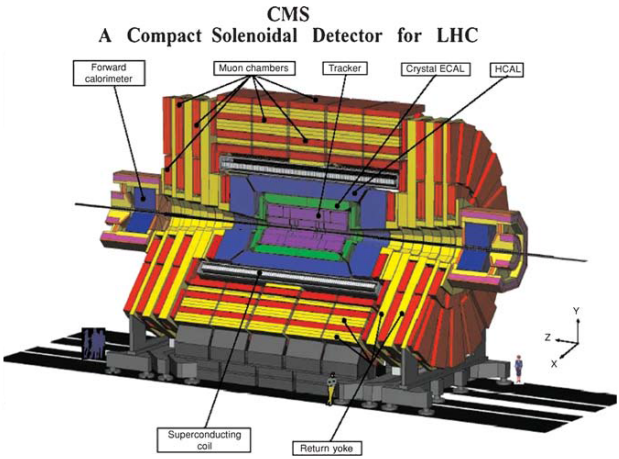

Figure 3.2: Structure of the CMS detector. [5]

3.1 Requirement

ATLAS and CMS are both designed to measure the collisions at the LHC as efficient and as precise as possible. With proton-proton collisions the strong interaction is involved, which will cause very complex final states and a very high backround because of confinement. In addition have the detectors to handle the high collision rate of 400MHz provided from the LHC and harsh radiation conditions near the interaction point, forcing the collaborations to work with radiation-hard materials.
Besides the collaborations had a finite budget to fund the studies, development and construction of their detectors, which made the whole project even more challenging. Superconducting technology was used for the detector magnets to limit the size and to lower the overall costs.

3.2 Structure

The structure of both ATLAS and CMS can be described as a cylinder with three different layers. The innermost layer is surrounded by a solendial magnetic field. The task of this layer is to measure the direction and momenta of all charged particles. This layer is called the tracker.
The second layer absorbs and measures the energy of electrons, photons and hadrons which is called the calorimetry system. It is partitioned in the EM (=*electromagnetic*) calorimeter for electrons and photons and in the hadron calorimeter.
The third and outer layer is the muon spectrometer. It measures the momenta and direction of high-energy muons.
The decisions which lead to this structures are driven by the methods used for the measurements and the elements of the detectors.
With a length of 46m and a diameter of 22m is ATLAS much larger than CMS which is just 20m long with a 15m diameter. Although CMS is smaller than ATLAS, it is with 12500 tons much heavier than ATLAS which just has a wheigt of 7000 tons.
Figures 3.1 and 3.2 show a sketch of ATLAS and CMS detectors. Illustrations about different particles crossing the different layers of the detectors are listed in the appendix (figures 5.1 and 5.2).

3.3 Magnet system

The magnet systems of both detectors provide the uniform magnetic field which is needed in the tracker and the muon spectrometer. The choice for the magnet system was mostly

driven by the measurement method of the muon system. CMS uses one single solenoid to create a high magnetic field (4T) in the tracker for all precision measurements, also muons. A high enough return flux in the iron yokes (see figure 3.2 yellow marked) outside the magnet provides a muon trigger and a second muon momentum measurement. The length of the solenoid was choosen to cover the required η coverage and the diameter to place tracker and most of the calorimetry inside the coil.
In contrast to CMS uses ATLAS more than one magnet. In the center we have a solenoid providing a 2T magnetic field for the tracker. Three large air-core toroids surrounding the calorimeter system provide the magnetic field for muon measurements. These are the two end-cap toroids situated at the front and the back of the calorimeters and the barrel toroid covering the calorimeters. The choice for this setup was driven by the requirement to perform high-precision stand-alone measurements of muons over an as large as possible momentum and η range. Having the calorimeter outside the coil leads to an impact on the EM calorimeter performance, so materials and diameters of the coil have been choosen to minimize performace losses. The length of the solenoid was choosen by the length of the calorimeter system and inner tracker system, resulting in a significant nonuniformity at the end of the tracker. The impact of the magnet system on the performance of the other detector elements will be discussed in the following sections.
Figure 3.3 shows a sketch of the ATLAS magnet system and table 3.1 shows the main parameters of the CMS and ATLAS magnet systems.

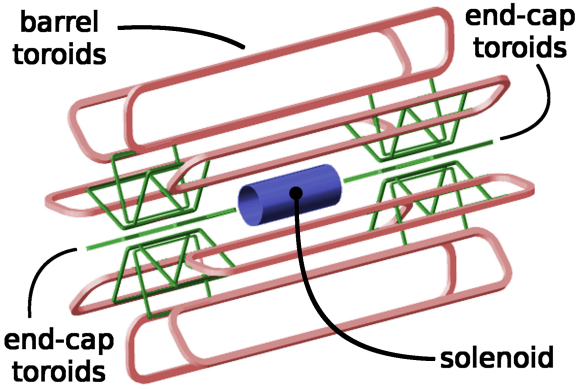

Figure 3.3: Structure of the ATLAS detector [8] (colors have been changed).

	CMS	ATLAS		
Parameter	**Solenoid**	**Solenoid**	**Barrel toroid**	**End-cap toroids**
Inner diameter	5.9 m	2.4 m	9.4 m	1.7 m
Outer diameter	6.5 m	2.6 m	20.1 m	10.7 m
Axial length	12.9 m	5.3 m	25.3 m	5.0 m
Number of coils	1	1	8	8
Number of turns per coil	2168	1173	120	116
Conductor size (mm^2)	64×22	30×4.25	57×12	41×12
Bending power	$4\ T \cdot m$	$2\ T \cdot m$	$3\ T \cdot m$	$6\ T \cdot m$
Current	19.5 kA	7.7 kA	20.5 kA	20.0 kA
Stored energy	2700 MJ	38 MJ	1080 MJ	206 MJ

Table 3.1: Main parameters of the CMS and ATLAS magnet system [5].

3.4 Inner tracker

The inner tracking system of ATLAS and CMS are designed to measure as precise and as efficient as possible the direction and momenta of all charged particles which emerge from the primary interaction with transverse momentum above about 1GeV and over a pseudorapitity range of $|\eta| < 2.5$.
Although there are harsh radiation conditions near the interaction point, the inner tracker needs to operate stable and robust over many years.
For ATLAS the inner tracker is situated into a fairly uniform 2T field while CMS provids a uniform 4T field, resulting in a better resolution for the inner tracker of CMS. Both detectors rely on silicon pixel and strip detectors for the inner tracker. Differences between the ATLAS and CMS silicon detectors are listed in table 3.2.

The interaction point is covered by three layers of pixel detectors for both ATLAS and CMS providing a set of three measurements per primary track. Details about the pixel detectors are found in the appendix (table 5.1)
At intermediate radii thin silicon strip detectors ($\approx 300\mu$m) are used by both experiments. For ATLAS this is called the SCT (*Semiconductor Tracker*) and is located between 30 and 60cm away from the interaction point. Between 20 and 55cm from the interaction point CMS has his TIB (*Tracker Inner Barrel*), TID (*Tracker Inner Disk*) and the first layer of the TEC (*Tracker End Cap*).
Between 55 and 107cm, CMS still uses silicon detectors in the TOB (*Tracker Outer Barrel*) and the TEC, making the inner tracker of CMS a full silicon tracker. These detectors are thicker ($\approx 500\mu$m and coarser pitches (120 to 180 μ). The whole tracker is cooled down to -10°C operation temperature to reduce the impact of radiation damage of the silicon detectors.
The pixel detectors and the SCT of the ATLAS are insulated and cooled down to operate at -7°C. Behind the SCT, between 56 and 107cm ATLAS uses the TRT (*Transition Radiation Tracker*) consisting of a set of 4 straw-tubes with 4mm in diameter which operate at room temperature using a Xe-CO_2-O_2 (79/27/3%) gas mixture. Due to finacial resons the TRT is limited to $|\eta| < 2$. In figure 3.4 and 3.5 are the inner tracker of ATLAS and CMS illustrated.

Parameter	ATLAS	CMS
Dimensions (cm)		
-radius of outermost measurement	101–107	107–110
-radius of innermost measurement	5.0	4.4
-total active length	560	540
Magnetic field B (T)	2	4
BR^2 ($T \cdot m^2$)	2.0 to 2.3	4.6 to 4.8
Total power on detector (kW)	70	60
Total weight in tracker volume (kg)	≈4500	≈3700
Total material (X/X_0)		
-at $\eta \approx 0$ (minimum material)	0.3	0.4
-at $\eta \approx 1.7$ (maximum material)	1.2	1.5
-at $\eta \approx 2.5$ (edge of acceptance)	0.5	0.8
Total material (λ/λ_0 at max)	0.35	0.42
Silicon microstrip detectors		
-number of hits per track	8	14
-radius of innermost meas. (cm)	30	20
-total active area of silicon (m^2)	60	200
-wafer thickness (microns)	280	320/500
-total number of channels	6.2×10^6	9.6×10^6
-cell size (μm in $R\phi \times$ cm in z/R)	80×12	$80/120 \times 10$
-cell size (μm in $R\phi \times$ cm in z/R)		and $120/180 \times 25$
Straw drift tubes (ATLAS only)		
-number of hits per track ($\lvert\eta\rvert < 1.8$)	35	
-total number of channels	350,000	
-cell size (mm in $R\phi \times$ cm in z)	4×70 (barrel) 4×40 (end caps)	

Table 3.2: Parameters of the CMS and ATLAS inner tracker elements [5]

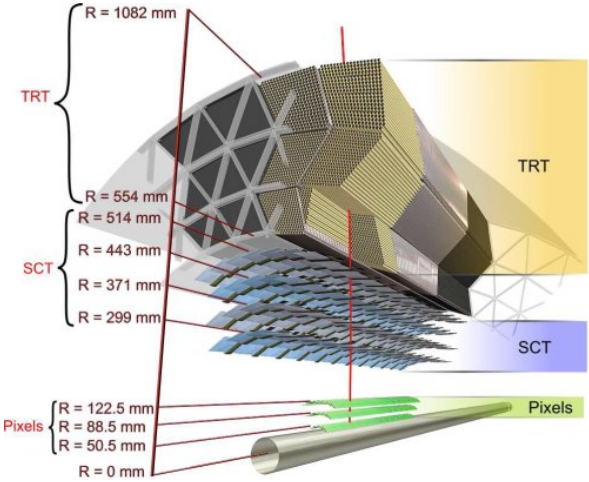

Figure 3.4: Sketch of the inner tracker of the ATLAS detector. It contains the pixel detector, the SCT and the TRT (barrel only) [6].

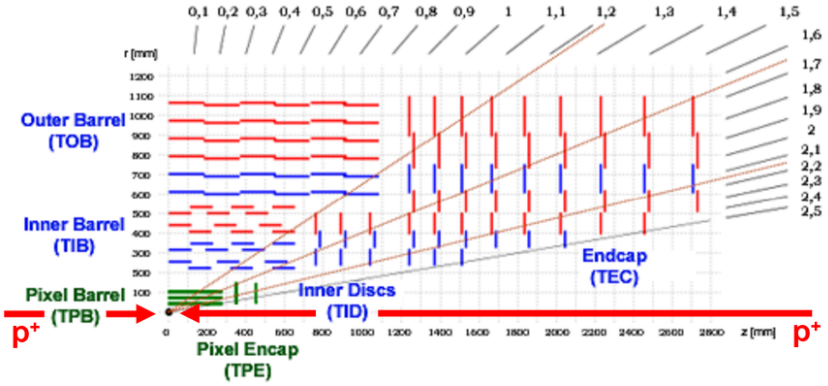

Figure 3.5: Profile of the CMS inner tracker [2].

3.5 Calorimeter system

For the calorimeter systems it is essentiel to have an excellent position and energy resolution over a wide pseudorapidety ($|\eta| < 2.5$) and energy range (few GeV to several TeV).

3.5.1 Electromagnetic calorimetry

The EM calorimeter of ATLAS and CMS consist of two parts. The barrel which covers approx. $|\eta| < 1.5$ and and two end-caps covering $1.4 < |\eta| < 3.2$ (3.0 for CMS). ATLAS relies on Lead/LAr (LAr=liquid Argon) accordion technology, which grants excellent lateral and longitudinal granularity. In contrast, CMS uses tungsten crystals ($PbWO_4$). These have no longitudinal segmentation but grant a fine lateral granularity and have a much better intinsic resolution then ATLAS EM calorimeter. Because the EM calorimeter of ATLAS is situated behind the solenoid, the photons and electrons already lose some energy in the solenoid which reduces the accuracy of the EM calorimeter measurements. The whole calorimeter system of ATLAS and CMS is shown in figure 3.6 and 3.7. Further information about the EM calorimeters are in table 5.2 (appendix).

3.5.2 Hadronic calorimetry

Between the hadronic calorimeters of ATLAS and CMS are serveral significant differences. In ATLAS we have the tile barrel and extended tile barrel using iron scintillating technology. These cover a range of $|\eta| <$1.5. Higher pseudorapidities are covered by the hadronic end-caps (HEC) and the forward calorimeter (FCAL). The end-caps are using copper and LAr

and cover a pseudorapidity of about $1.5 < |\eta| < 3$. The FCAL is installed inside the HEC and covers $3 < |\eta| < 5$ and is built of copper (front)/ tungesten(back) and LAr.
The CMS hadron calorimeter is seperated into barrel, end caps and forward calorimeter. These cover about the same pseudorapidity like the ATLAS hadron calorimeter parts. Both barrel and end-caps use brass/scintillator technology. For the forward calorimeter steel is used.
One important difference between ATLAS and CMS is, that the CMS calorimeters are situated inside the solenoid, causing spatial limitations for the calorimeters. Because of these spatial limitations has the hadronic calorimeter of CMS insufficient absorbtion of hadrons. To protect the muon chambers from punch-through, a tail-catcher was added which stops but not measures hadrons, making it through the calorimeter. This results in a reduced resolution.

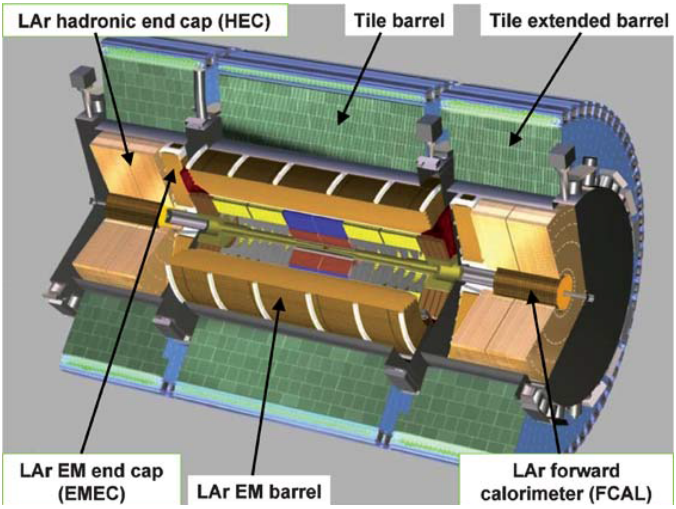

Figure 3.6: Sketch of the ATLAS calorimeter system [5].

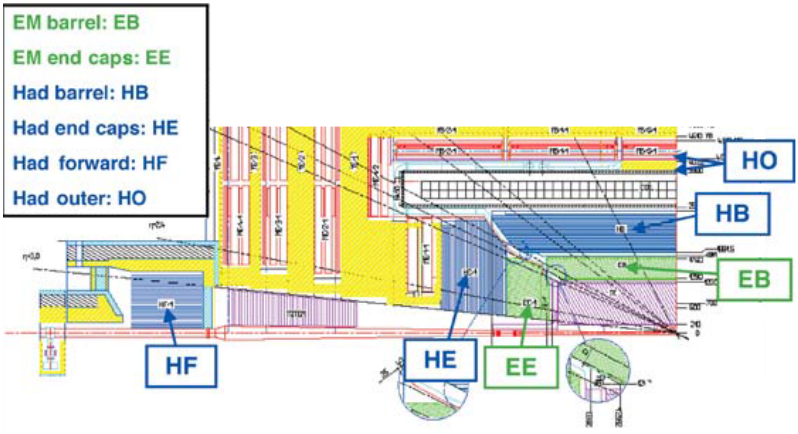

Figure 3.7: Profile of the CMS calorimeter system [5].

3.6 Muon spectrometer system

Both ATLAS and CMS were mostly shaped by the decision made for the muon systems. This is because muons are very robust and deliver a clean and unambiguous signatures for the higgs search (like $H \rightarrow ZZ \rightarrow 4\mu$).
ATLAS decided on a high-resolution, stand-alone measurement which is independent of the other detector parts. This resulted in a detector with large volume and low density. In contrast, CMS uses the concept of a compact detector. To reach enough bending power for the muon measurement a high magnetic field is necessary.
ATLAS uses 4 kind of muon detectors. Monitored drift tubes (MDTs) and cathode strip chambers (CSCs) for precision measurement, resistive plate chambers (RPCs) and thin gap chambers (TGCs) for triggering. In the barrel region the MDTs and RPCs are used and cover a pseudorapidety of $|\eta| <1.05$. The MDTs are also used in the end-cap region enhancing the range to $|\eta| <2$ and. For larger $|\eta|$ is the neutron-induced backround and muon hit rate much higher. In this region CSCs are used covering $2.0 < |\eta| < 2.7$. TGCs are assuming the triggering in the end-cap region and cover therefore a pseudorapidity of $1.05 < |\eta| < 2.4$. A profile of the ATLAS and CMS muon system with the different layers is shown in figure 3.8.
CMS decided to use only 3 different elements for their muon spectrometer. Drift tubes, CSCs and RPCs. Their tasks is both precision measurement and triggering, expect the RPCs which are used for triggering alone. Like ATLAS uses CMS both drift tubes and RPCs in the barrel region covering $|\eta| <1.2$. However CMS extendend the RPCs to the end-cap region enhancing their range to $|\eta| <2.1$. The CSCs are also used in regions with harsher backround and muon hit rate conditions,

covering $1.2 < |\eta| < 2.4$. Table 5.3 shows a detailed comparison between the ATLAS and CMS muon chambers.

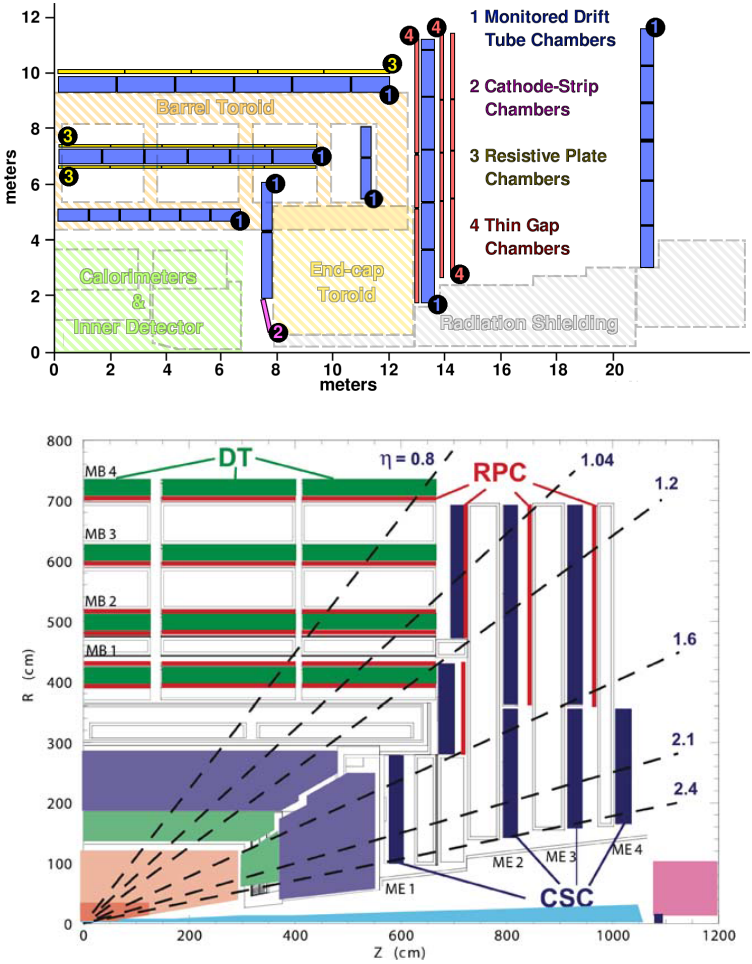

Figure 3.8: Sketch of the different layers of the ATLAS (above [7]) and CMS (below [5]) muon spectrometer.

4 Performance

To obtain results from the data obtained from ATLAS and CMS, excellent knowledge of the detector performance is essential. Extensive test-beam measurements and simulations had been done over years to obtain knowledge about the resolution and efficiency of the detector components.

4.1 Inner tracker

	ATLAS	CMS
Reconstruction efficiency for muons with $p_T = 1$ GeV	96.8%	97.0%
Reconstruction efficiency for pions with $p_T = 1$ GeV	84.0%	80.0%
Reconstruction efficiency for electrons with $p_T = 5$ GeV	90.0%	85.0%
Momentum resolution at $p_T = 1$ GeV and $\eta \approx 0$	1.3%	0.7%
Momentum resolution at $p_T = 1$ GeV and $\eta \approx 2.5$	2.0%	2.0%
Momentum resolution at $p_T = 100$ GeV and $\eta \approx 0$	3.8%	1.5%
Momentum resolution at $p_T = 100$ GeV and $\eta \approx 2.5$	11%	7%
Transverse i.p. resolution at $p_T = 1$ GeV and $\eta \approx 0$ (μm)	75	90
Transverse i.p. resolution at $p_T = 1$ GeV and $\eta \approx 2.5$ (μm)	200	220
Transverse i.p. resolution at $p_T = 1000$ GeV and $\eta \approx 0$ (μm)	11	9
Transverse i.p. resolution at $p_T = 1000$ GeV and $\eta \approx 2.5$ (μm)	11	11
Longitudinal i.p. resolution at $p_T = 1$ GeV and $\eta \approx 0$ (μm)	150	125
Longitudinal i.p. resolution at $p_T = 1$ GeV and $\eta \approx 2.5$ (μm)	900	1060
Longitudinal i.p. resolution at $p_T = 1000$ GeV and $\eta \approx 0$ (μm)	90	22–42
Longitudinal i.p. resolution at $p_T = 1000$ GeV and $\eta \approx 2.5$ (μm)	190	70

Table 4.1: [5].

Table 4.1 shows the main performance characteristics of both ATLAS and CMS inner trackers.
Regarding the momentum resolution the CMS tracker is superior to the ATLAS tracker. This is not surprising since the CMS detector provides a more uniform magnetic field for the inner tracker. However ATLAS has a slightly better reconstruction efficieny, which is due to the lower magnetic field in the tracker because high magnetic fields enhance effects of interactions in the detector material. The resolution of the impact parameter is similar in the transverse plane but slightly different in favor of CMS in the longitudinal plane. In the longitudinal plane the small CMS pixel size leads to a better resolution. However in transversal plane the pixel size of ATLAS is smaller but gets countered by charge-sharing pixels next to each other and the analog readout of the CMS pixel system.

4.2 Calorimeter system

EM calorimeter
For photons with an energy of 100Gev the expected ATLAS energy resolution is about 1.19% for unconverted photons and 1.44% for converted photons. For CMS there is an overall expected resolution of just 0.75% which is due to the high intrinsic resolution of the used tungsten crystals. Also the ATLAS EM calorimeter is situated outside of the solenoid which causes some reduced resolution.
For electrons with 50GeV the resolution varies between 1.3% ($|\eta| = 0.3$) and 1.8% ($|\eta| = 1.1$) for the ATLAS EM calorimeter independent of the tracker. CMS just has an estimated resolution of 2%. Because ATLAS has both a good lateral

and longitudinal granularity and CMS has just a good lateral granularity, the resolution independent of tracker informations is lower for CMS than for ATLAS. The dependency of the resolution for photons and electrons with their energy is shown in figure 4.1.

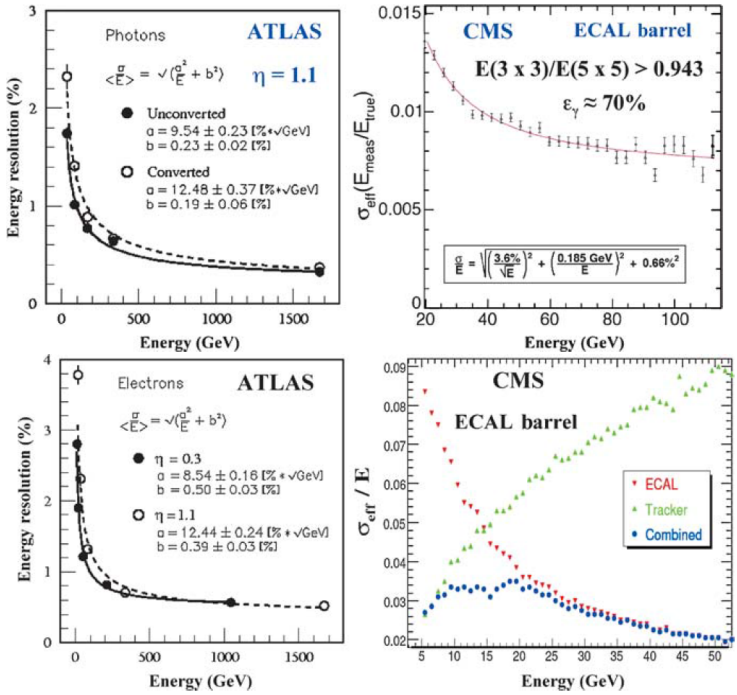

Figure 4.1: Top is the expected relative precision of the energy measurement of photons. On the bottom there is the same for electrons. [5]

Hadronic calorimeter

Regarding the performance, the main difference of the hadronic calorimeters of ATLAS and CMS is that the CMS has insufficient absorption and was forced to use a tail-catcher.. Figure 4.2 shows the expected energy resolution of QCD jets.

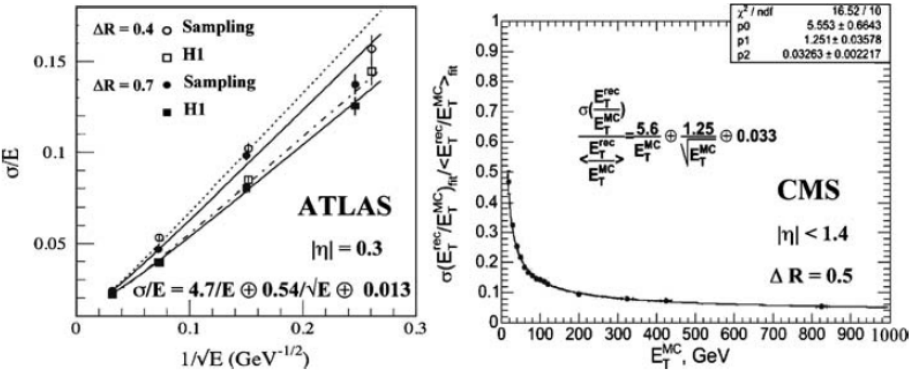

Figure 4.2: Energy resolution of jets reconstructed in the central region. For ATLAS as a function of $1/\sqrt{E}$ with E as the jet energy and for CMS as a function of E_T^{MC} (=transverse energy of jet)[5]

For jets with 1TeV atals reaches about 2% resolution whereas CMS just has an expected resoltution of 5%. ATLAS is also superior in the measurement of the missing transverse resoltuion. Figure 4.3 shows the precision of the missing transverse energy (σ)as a function of the total missing transversal energy (ΣE). For a total missing transversal energy of 2TeV ATLAS has a precision of $\sigma \approx 20$ and CMS nearly double as much with $\sigma \approx 40$.

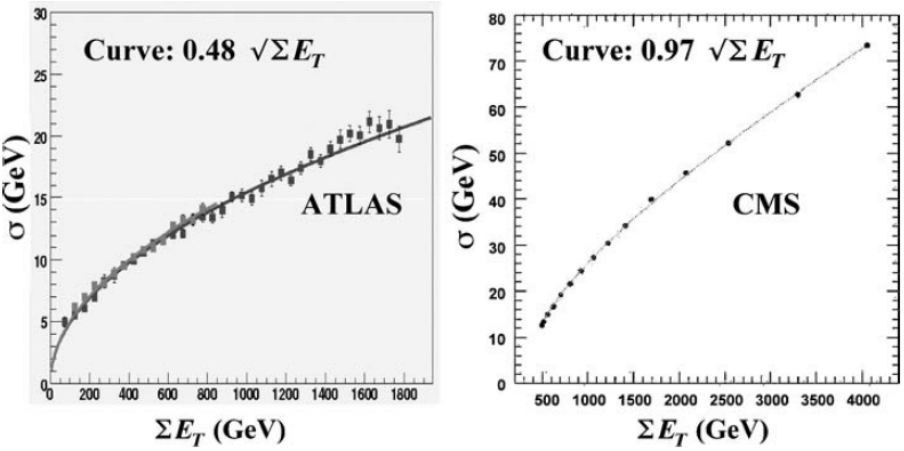

Figure 4.3: The expected missing transersal resolution as a function of the total missing transversal energy [5]

4.3 Muon spectrometer system

The following table 4.2 shows the performance of the ATLAS and CMS myon system.

Parameter	ATLAS	CMS
Pseudorapidity coverage		
-Muon measurement	$\|\eta\| < 2.7$	$\|\eta\| < 2.4$
-Triggering	$\|\eta\| < 2.4$	$\|\eta\| < 2.1$
Dimensions (m)		
-Innermost (outermost) radius	5.0 (10.0)	3.9 (7.0)
-Innermost (outermost) disk (z-point)	7.0 (21–23)	6.0–7.0 (9–10)
Segments/superpoints per track for barrel (end caps)	3 (4)	4 (3–4)
Magnetic field B (T)	0.5	2
-Bending power (BL, in T· m) at $\|\eta\| \approx 0$	3	16
-Bending power (BL, in T· m) at $\|\eta\| \approx 2.5$	8	6
Combined (stand-alone) momentum resolution at		
-p = 10 GeV and $\eta \approx 0$	1.4% (3.9%)	0.8% (8%)
-p = 10 GeV and $\eta \approx 2$	2.4% (6.4%)	2.0% (11%)
-p = 100 GeV and $\eta \approx 0$	2.6% (3.1%)	1.2% (9%)
-p = 100 GeV and $\eta \approx 2$	2.1% (3.1%)	1.7% (18%)
-p = 1000 GeV and $\eta \approx 0$	10.4% (10.5%)	4.5% (13%)
-p = 1000 GeV and $\eta \approx 2$	4.4% (4.6%)	7.0% (35%)

Table 4.2: Main parameters of the ATLAS and CMS muon spectrometers. Also the stand-alone and combined momentum resolution is shown for different momenta [5].

We see that ATLAS covers a larger pseudorapidety than CMS. Regarding the resolution of the muon momentum CMS has a better combined performance whereas ATLAS has excellent stand-alone measurements, which it was designed for.

5 Appendix

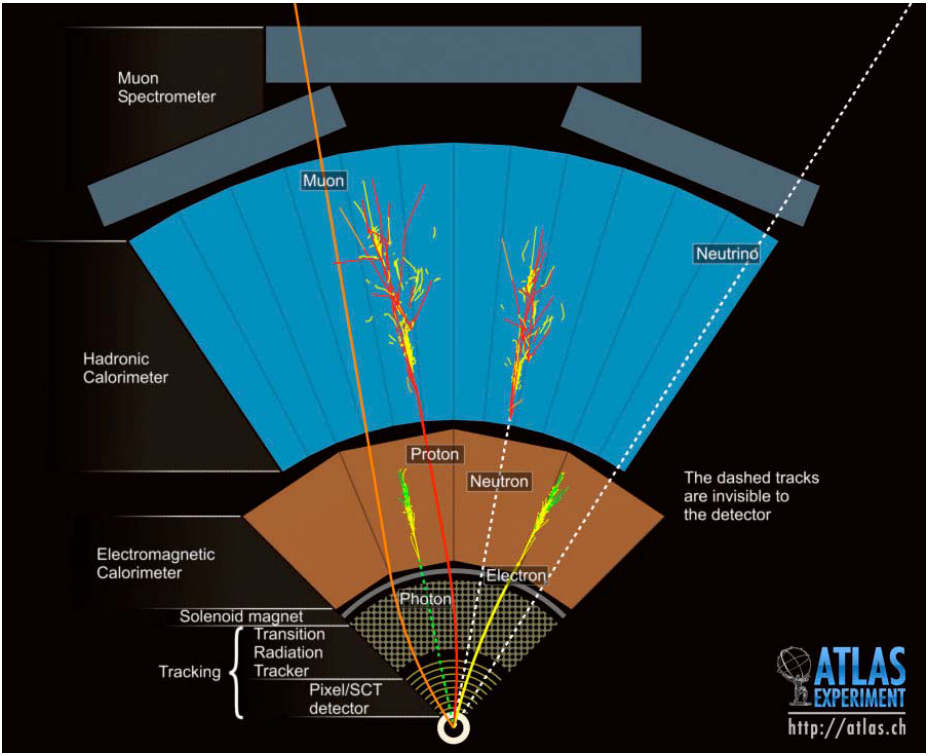

Figure 5.1: Sketch of the different layers the ATLAS.

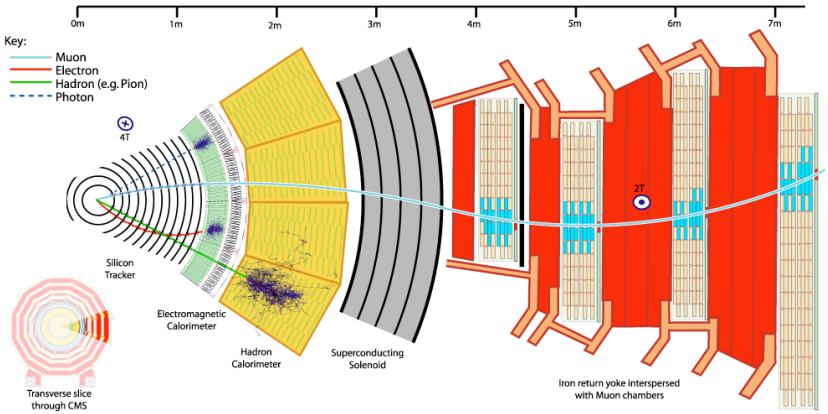

Figure 5.2: Sketch of the different layers the CMS detector [1].

	CMS	ATLAS		
Parameter	**Solenoid**	**Solenoid**	**Barrel toroid**	**End-cap toroids**
Inner diameter	5.9 m	2.4 m	9.4 m	1.7 m
Outer diameter	6.5 m	2.6 m	20.1 m	10.7 m
Axial length	12.9 m	5.3 m	25.3 m	5.0 m
Number of coils	1	1	8	8
Number of turns per coil	2168	1173	120	116
Conductor size (mm^2)	64×22	30×4.25	57×12	41×12
Bending power	$4\ T \cdot m$	$2\ T \cdot m$	$3\ T \cdot m$	$6\ T \cdot m$
Current	19.5 kA	7.7 kA	20.5 kA	20.0 kA
Stored energy	2700 MJ	38 MJ	1080 MJ	206 MJ

Table 5.1: Main parameters of the CMS and ATLAS magnet system [5].

Main parameters of the ATLAS and CMS electromagnetic calorimeters

	ATLAS		**CMS**	
Technology	Lead/LAr accordion		$PbWO_4$ scintillating crystals	
Channels	Barrel	End caps	Barrel	End caps
	110,208	63,744	61,200	14,648
Granularity	$\Delta\eta \times \Delta\phi$		$\Delta\eta \times \Delta\phi$	
Presampler	0.025×0.1	0.025×0.1		
Strips/ Si-preshower	0.003×0.1	0.003×0.1 to 0.006×0.1		32×32 Si-strips per 4 crystals
Main sampling	0.025×0.025	0.025×0.025	0.017×0.017	0.018×0.003 to 0.088×0.015
Back	0.05×0.025	0.05×0.025		
Depth	Barrel	End caps	Barrel	End caps
Presampler (LAr)	10 mm	2×2 mm		
Strips/ Si-preshower	$\approx 4.3\ X_0$	$\approx 4.0\ X_0$		$3\ X_0$
Main sampling	$\approx 16\ X_0$	$\approx 20\ X_0$	$26\ X_0$	$25\ X_0$
Back	$\approx 2\ X_0$	$\approx 2\ X_0$		
Noise per cluster	250 MeV	250 MeV	200 MeV	600 MeV
Intrinsic resolution	Barrel	End caps	Barrel	End caps
Stochastic term a	10%	10 to 12%	3%	5.5%
Local constant term b	0.2%	0.35%	0.5%	0.5%

Table 5.2: Table from [5].

	ATLAS	CMS
Drift Tubes	MDTs	DTs
-Coverage	$\|\eta\| < 2.0$	$\|\eta\| < 1.2$
-Number of chambers	1170	250
-Number of channels	354,000	172,000
-Function	Precision measurement	Precision measurement, triggering
Cathode Strip Chambers		
-Coverage	$2.0 < \|\eta\| < 2.7$	$1.2 < \|\eta\| < 2.4$
-Number of chambers	32	468
-Number of channels	31,000	500,000
-Function	Precision measurement	Precision measurement, triggering
Resistive Plate Chambers		
-Coverage	$\|\eta\| < 1.05$	$\|\eta\| < 2.1$
-Number of chambers	1112	912
-Number of channels	374,000	160,000
-Function	Triggering, second coordinate	Triggering
Thin Gap Chambers		
-Coverage	$1.05 < \|\eta\| < 2.4$	—
-Number of chambers	1578	—
-Number of channels	322,000	—
-Function	Triggering, second coordinate	—

Table 5.3: Main parameters of the CMS and ATLAS muon system [5].

Bibliography

[1] Cms experiment. http://cms.web.cern.ch/news/how-cms-detects-particles.

[2] Institute for high-energy physics. http://www.hephy.at/forschung/projekte/cms-inner-tracker/.

[3] Aglietti, U., Belyaev, A., Berge, S., Blum, A., Bonciani, R., Cammin, J., Carena, M., Chivukula, S., Davoudiasl, H., Dawson, S., Degrassi, G., Dominguez, A., Donini, J., Dorigo, T., Field, B., Hahn, T., Han, T., Heinemeyer, S., Hesselbach, S., Huang, G.-Y., Iashvilli, I., Jackson, C., Junk, T., Lee, S.-W., Logan, H., Maltoni, F., Mellado, B., Moretti, S., Mrenna, S., Nadolsky, P., Olness, F., Quayle, W., Rathsman, J., Reina, L., Simmons, E., Sopczak, A., Vicini, A., Wackeroth, D., Wagner, C., Weiglein, G., Weiglein, G., Willenbrock, S., Wu, S., and Yuan, C. Tevatron-for-lhc report:higgs. *Cornell University Library http://arxiv.org/abs/hep-ph/0612172*.

[4] Bruenning, O., Burkhardt, H., and Myers, S. The large hadron collider. *Progress in Particle and Nuclear Physics 67* (2012), 705–734.

[5] Froidevaux, D., and Sphicas, P. General-purpose detectors for the large hadron collider. *Annu. Rev. Nucl. Part. Sci. 56* (2006), 375–440.

[6] FSP101-ATLAS. http://www.fsp101-atlas.de/e197881/e200172/.

[7] Goodson, J. *Search for Supersymmetry in States with Large Missing Transverse Momentum and Three Leptons including a Z-Boson*. PhD thesis, Stony Brook University, May 2012. Presented 17 Apr 2012.

[8] Ruber, R. Atlas magnet group. http://atlas-ma.web.cern.ch/atlas-ma/images/atlas-ma.gif.

[9] Schumacher, M. Lecture: Hadron collider physics. University of Freiburg, 2014.